RESEARCH ARTICLE

Mechanism for corrosion protection of β-TCP reinforced ZK60 *via* laser rapid solidification

Youwen Deng[1#], Youwen Yang[2#], Chengde Gao[2], Pei Feng[2], Wang Guo[2], Chongxian He[2], Jian Chen[1], Cijun Shuai[2,3,4*]

[1] Department of Emergency Medicine, the Second Xiangya Hospital, Central South University, Changsha, China
[2] State Key Laboratory of High Performance Complex Manufacturing, Central South University, Changsha, China
[3] Jiangxi University of Science and Technology, Ganzhou, China
[4] Key Laboratory of Organ Injury, Aging and Regenerative Medicine of Hunan Province, Changsha, China

Abstract: It remains the primary issue to enhance the corrosion resistance of Mg alloys for their clinical applications. In this study, β-tricalcium phosphate (β-TCP) was composited with Mg-6Zn-1Zr (ZK60) using laser rapid solidification to improve the degradation behavior. Results revealed rapid solidification effectively restrained the aggregation of β-TCP, which thus homogenously distributed along grain boundaries of α-Mg. Significantly, the uniformly distributed β-TCP in the matrix promoted the formation of apatite layer on the surface, which contributed to the formation of a compact corrosion product layer, hence retarding the further degradation. Furthermore, ZK60/8β-TCP (wt. %) composite showed improved mechanical strength, as well as improved cytocompatibility. It was suggested that laser rapidly solidified ZK60/8β-TCP composite might be a potential materials for tissue engineering.

Keywords: laser rapid solidification; ZK60/β-TCP composite; degradation behavior; microstructure

*Correspondence to: Cijun Shuai, State Key Laboratory of High Performance Complex Manufacturing, Central South University, Changsha 410083, China; shuai@csu.edu.cn
#These authors contributed equally to this work.

Received: September 29, 2017; **Accepted**: November 6, 2017; **Published Online**: November 21, 2017

Citation: Deng Y, Yang Y, Gao C, *et al*., 2018, Mechanism for corrosion protection of β-TCP reinforced ZK60 *via* laser rapid solidification. *Int J Bioprint*, 4(1): 124. http://dx.doi.org/10.18063/IJB.v4i1.124

1. Introduction

Magnesium (Mg) alloys have been considered as a new generation of degradable implant materials due to their inherent biofiguredegradability and appropriate mechanical properties[1]. Mg, as one of the essential elements in body, participates in a large number of metabolic reactions, especially in bone metabolism[2]. There have been extensive studies on various Mg alloys as absorbable biomaterials, including AZ31 (Mg-based alloy with 3% Al 1% Zn)[3], WE[4] and Mg-6Zn-1Zr (ZK60) alloys[5]. Among these, ZK60 presents superior strength and good biocompatibility, attracting great attention for its applications in tissue engineering[6]. Unfortunately, ZK60 degrades too rapidly in internal environments, resulting in severe problems including excessive inflammatory response, hydrogen gas accumulation, alkalization of body fluids and premature mechanical failure[7].

Recently, enforcement by utilizing bioceramic materials has been reported to be an effective method to enhance the corrosion resistance of Mg alloys. For example, Campo *et al*.[8] reported that Mg-HAP exhibited improved corrosion resistance compared with Mg. Wan *et al*.[9] also reported that the addition of 45s bioglass into Mg significantly reduced the corrosion rate for Mg. Feng and Han[10] fabricated Mg-based composites reinforced with calcium polyphosphate, which exhibited controllable degradation rates. However, previous study also revealed that the incorporated bioceramic easily segregated together in the Mg matrix even at a low content. He *et al*.[11] observed the agglomeration of tricalcium phosphate (TCP) particles occurred in as-extruded Mg-3Zn-0.8Zr/1.5TCP (wt. %). Liu *et al*.[12] investigated microstructure of the as-casted Mg–3Zn–1Ca/1β-TCP (wt. %), also revealing the agglomeration of the β-TCP particles in the sample. It is well known that the agglomeration of incorporated bioceramic can cause the formation of pores and defects, thus deteriorating the corrosion behavior and mechanical properties of Mg

matrix. Meanwhile, the conventional processes, also including powder metallurgy[13], are difficult to prepare porous Mg alloys with complex shapes.

In the present study, laser melting technology is proposed to overcome the agglomeration of incorporated bioceramic. Laser melting technology is a typical rapid solidification which has an extremely high cooling rate over 10^5 K/s, which allows the solidification can be completed in an extremely short period of time[14]. In this condition, the ceramic particles which originally uniformly dispersed in the liquid pool cannot agglomerate in such a short time, thus homogenously distributing in the matrix. Meanwhile, the rapid solidification is able to refine the microstructure, which is also beneficial to enhance the corrosion resistance of Mg alloys[15]. Another study on Ti–TiB composites further confirmed that laser melting was an effective method that could produce almost fully dense composites with bioceramic enforcement[16]. On the other hand, laser melting technology can fabricate porous Mg alloys[17]. To the best of our best knowledge, there are few publications studying on the corrosion behavior of laser rapidly solidified biocaremic reinforced Mg alloys.

In this study, β-TCP was introduced to ZK60 to improve its degradation behavior *via* laser rapid solidification. β-TCP had good bioactivity as well as good wettability with the Mg alloy[18]. ZK60/β-TCP composites with different contents of β-TCP (0–12 wt. %) were prepared. And the microstructure features, degradation behavior and mechanical properties were investigated.

2. Materials and Methods

2.1 Materials

β-TCP powder with a size of approximately 200 nm (Figure 1A) was obtained from Kunshan Chinese Technology New Materials Co. Ltd., China. Spherical ZK60 powder was purchased from Tangshan Weihao Materials Co. Ltd., China. The chemical composition was as follows: 6.63 wt. % of Zn, 0.56 wt. % of Zr and balanced Mg. The size of the ZK60 powder was <50 μm (Figure 1B). The ZK60 alloy powder was composited with 0, 4, 8 and 12 wt. % of β-TCP powder, respectively, followed by ball milling under a protective gas (0.3 vol. % SF_6 and 99.7 vol. % CO_2) at a rotation speed of 150 rpm. After ball milling for 2 h, the small β-TCP particles uniformly adhered to the surface of large ZK60 particles (Figure 1C and Figure 1D). The homogeneity of the powder could improve the flowability and allow for improved packing of powder, thus reducing the formation of defects[19].

2.2 Fabrication of the Composites

The ZK60/*x*β-TCP (*x* = 0, 4, 8 and 12 wt. %) composites were fabricated by a home-made laser melting system, which comprised of a powder delivery device, a three-dimensional motion platform and a fiber laser[17]. In the laser melting process, a high energy laser beam scanned the powder layer, forming a solid layer. Then, the formed solid layer was covered with a new layer of powder. The cycle continued before the samples (8×8×8 mm^3) were achieved. The samples were fabricated at a laser power of 80 W, a scanning rate of 300 $mm \cdot s^{-1}$ and a layer thickness of 0.1 mm. All procedures were performed under a protective argon atmosphere.

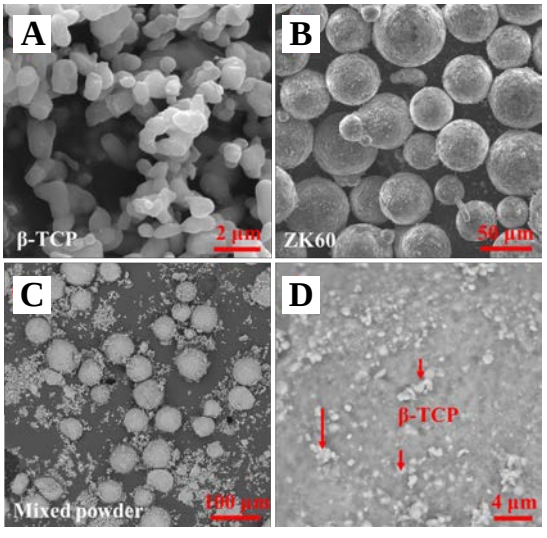

Figure 1. Original powders: (**A**) β-TCP powder; (**B**) ZK60 powder; (**C**) ZK60/8β-TCP (wt. %) mixed powder; and (**D**) the surface on ZK60 particle in mixed powder.

2.3 Microstructure Characterization

The microstructure was analyzed by scanning electron microscopy (SEM; JSM-5600LV, Japan). The sample was prepared as follows: the ZK60/*x*β-TCP composites were successively grounded with abrasive papers (500, 1000 and 2000 grit), and polished with diamond grits. The phase composition of the composites was identified using an X-ray diffractometer (XRD, D8-Advance, Germany). The condition was set using Cu Kα radiation at 15 mA and 30 kV. Scans were performed with 2θ range of 5° to 80° at a scanning rate of 8°·min^{-1}.

The relative density of the laser rapidly solidified composites was studied using Image-Pro Plus 6.0 software. After grinded and polished, optical micrographs of each sample were obtained. The obtained optical micrographs were then turned into the gray mode. A proper threshold value of gray scale was determined as gray scale of the pores. Then, the area percentage of pores was obtained by calculating the area ratio of the marked regions to the whole micrograph. Triplicate tests were conducted for each sample.

2.4 Immersion Test

The immersion experiments were conducted to access the corrosion behavior of the ZK60/*x*β-TCP composites. Simulated body fluid (SBF) served as the degradation medium. The pH variations of the SBF were recorded during the immersion for 10 days. In addition, the corrosion surface of the composites was observed by SEM after immersion for 7 days. The chemical composition was analyzed by energy dispersive spectroscopy (EDS, JSM-5910LV, Japan). Weight loss method was used to obtain the quantified data on the degradation behavior of Mg-based composite. The weight of the samples after the corrosion test was measured after removal of the corrosion products in chromic acid. An average of three measurements was taken for each group. The *in vitro* corrosion rate was calculated according to the equation:

$$C = M_{loss}/(qAT)$$

where C was the corrosion rate in mm/year, M_{loss} was the weight loss, q was the density of the material, A was the initial immersion surface area and T was the immersion time.

2.5 Mechanical Properties

The compressive strength was assessed by a universal testing machine (WD-01, Shanghai Zhuoji instruments Co. Ltd., China) at a loading rate of 0.5 mm·min^{-1}. The test samples with the size of 3×3×6 mm^3 were prepared according to the ASTM-E9-09. Three identical samples were used for the compressive tests. Besides, indentation tests were performed to evaluate the hardness of the composite by a hardness tester (Taiming Optical Instrument Corporation, China). The applied load and loading time were 0.98 N and 15 seconds, respectively. Triplicate tests were conducted for each sample.

2.6 *In Vitro* Cell Culture

MG-63 cells were used for the *in vitro* cell culture. Dulbecco's modified eagle medium (DMEM) with 10% fetal bovine serum, 100 U·mL^{-1} penicillin and 100 mg·mL^{-1} streptomycin were used as culture medium. ZK60/*x*β-TCP samples were immersed in DMEM for 3 days to prepare extracts (surface area to extracts volume 1.25 cm^2·mL^{-1}) in humidified atmosphere (5% CO_2, 37 °C).

MG-63 cells were first cultured in DMEM in a 24-well plate. After 4 h, the cell culture media were substituted by previously prepared extracts. Cells were cultured in a humidified atmosphere for 1 day (5% CO_2, 37 °C). Subsequently, the cells were gently rinsed with phosphate buffered saline (PBS) and then stained with Calcein-AM and Ethidium homodimer-1 reagents (15 min, 37 °C). After gently rinsing with PBS, the specimens were mounted onto glass slides and then observed by fluorescence microscopy (BX60, Olympus, Japan).

Besides, CCK-8 assay was used to assess cell viability of MG-63 cells cultured in extracts of ZK60/*x*β-TCP composites. The MG-63 cells were seeded onto the 96-well plate (cells density 1×10^5 per mL) and cultured for 1 day. Then, the cell culture media were substituted by prepared extracts, with DMEM serving as control. After cultured for 1, 3 and 5 days, cells were incubated with 10 μL CCK-8 (5 mg/mL, Sigma-Aldrich, St. Louis, MO, USA) for 2 h, then the absorbance was measured at 450 nm by paradigm detection platform (BECK MAN, S. Kraemer Boulevard Brea, CA). The obtained optical density (O.D.) values were proportional to the live cell numbers.

2.7 Statistical Analysis

Quantitative data were presented as mean ± standard deviation, and analyzed using the STATA (Data Analysis and Statistical Software). Statistical significance was defined when the p-value was <0.05.

3. Results and Discussion

3.1 Microstructure

The typical microstructures of the laser rapidly solidified ZK60/*x*β-TCP composites were presented in Figure 2. For ZK60, only a small amount of second phases (MgZn intermetallic phase) distributed in Mg matrix (Figure 2A). After composited with 4 wt. % β-TCP, divorced slender

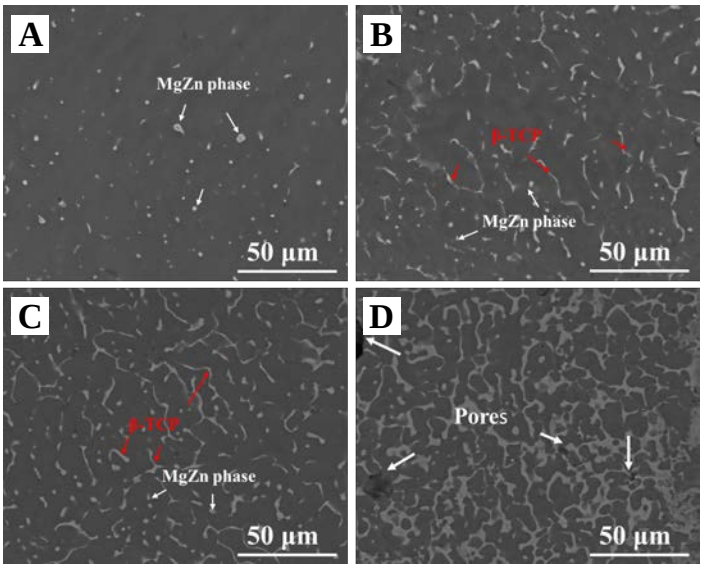

Figure 2. SEM of the ZK60/xβ-TCP composites: (**A**) dot like MgZn phase distributed in ZK60; (**B**) divorced slender β-TCP phase uniformly distributed along grains boundaries in ZK60/4β-TCP; (**C**) continuous slender β-TCP phase in ZK60/8β-TCP; (**D**) pores were observed in ZK60/12β-TCP.

β-TCP phase was observed uniformly distributing along grains boundaries (Figure 2B). For ZK60/8β-TCP, more slender β-TCP phases homogeneously precipitated along the grain boundaries, compared with ZK60/4β-TCP (Figure 2C). While β-TCP content was up to 12 wt. %, the precipitated β-TCP was considerably coarsened and agglomerated, forming a continuous network structure. Besides, some pores were observed in the matrix of ZK60/12β-TCP (Figure 2D).

The relative density of laser-melted ZK60/*x*β-TCP composites was investigated, with results shown in Figure 3. Laser-melted ZK60 obtained a high level of relative density of 98.8 ± 0.6%. After composited with β-TCP, ZK60/4β-TCP and ZK60/8β-TCP still reached a high relative density of 97.6 ± 1.1% and 97.2 ± 1.8%, respectively, with no significant difference among ZK60, ZK60/4β-TCP and ZK60/8β-TCP ($p > 0.05$). However, a considerable decrease of relative density to 88.5 ± 3.5% was observed with a further increase of β-TCP to 12 wt. %. The significantly lower relative density of ZK60/12β-TCP as compared with ZK60/8β-TCP indicated that the agglomeration of β-TCP particles deteriorated the densification behavior of Mg matrix during solidification.

The obtained XRD patterns of β-TCP/ZK60 composites were shown in Figure 4. Compared with the ZK60, besides the diffraction peaks corresponding to α-Mg, the diffraction peaks of β-TCP were also detected in the β-TCP/*x*ZK60 composite. In addition, the diffraction peaks of β-TCP became stronger with β-TCP increasing. The XRD results also demonstrated that no other new phases formed, indicating that no chemical

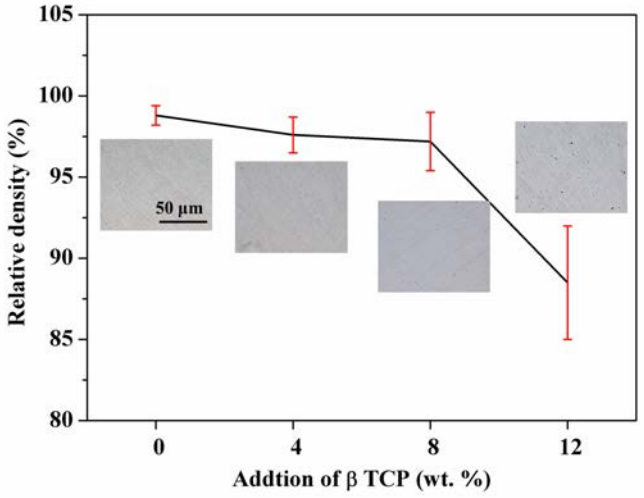

Figure 3. The relative density of the ZK60/xβ-TCP composites. The insets were the corresponding optical images.

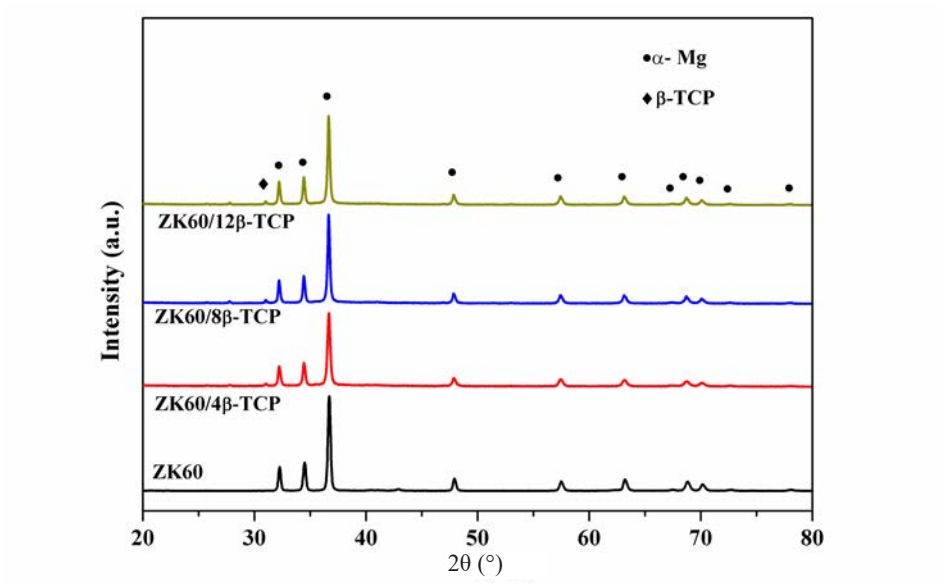

Figure 4. XRD patterns of the ZK60/xβ-TCP composites

reactions occurred between β-TCP and Mg alloys during the laser melting.

3.2 Mechanical Properties

The obtained compressive strength of laser-melted ZK60/*x*β-TCP composites was shown in Figure 5A. ZK60 exhibited a relatively low compressive strength of 111.8 ± 6.8 Mpa. After composited with 8 wt. % β-TCP, the compressive strength was gradually improved to 207.4 ± 7.7 Mpa. However, a further increase of β-TCP to 12 wt. % resulted in a dramatically decrease of compressive strength to 167.4 ± 12.2 Mpa. Besides, the hardness of the laser rapidly solidified ZK60/β-TCP composites was also obtained, with results shown in Figure 5B. It could be observed that the hardness of ZK60/*x*β-TCP composites significantly increased with β-TCP increasing. ZK60 exhibited a low hardness of 82.4 ± 3.8 HV, while ZK60/4β-TCP, ZK60/8β-TCP and ZK60/12β-TCP had an enhanced hardness of 97.6 ± 4.5 Hv, 127.2 ± 5.7 Hv and 153.4 ± 12.2 Hv, respectively.

3.3 Degradation Behavior

The degradation behavior of the ZK60/*x*β-TCP composites was evaluated by immersion tests in SBF. Moreover, the pH variation of the SBF for ZK60/*x*β-TCP composites as a function of soaking time was presented in Figure 6A. It could be seen that the pH values of SBF for different composites had similar change tendency during the immersion period, increasing quickly at the first 48 h and stabilizing during further immersion. After immersed for 240 h, the obtained pH value of SBF for ZK60/8β-TCP exhibited a lowest value of 9.42 ± 0.09, as compared with SBF for ZK60 (10.25 ± 0.12), ZK60/4β-TCP (9.73 ± 0.13) and ZK60/12β-TCP (10.69 ± 0.10). The increase of pH value was due to the generation of OH^- resulting from the degradation of Mg. Thus, it was indicated that ZK60/8β-TCP showed the highest corrosion resistance. The corrosion rates of the ZK60/*x*β-TCP composites were calculated based on weight loss (Figure 6B). Clearly, ZK60/8β-TCP showed a decreased corrosion rate of 0.58 ± 0.11 mm/year, as compared with ZK60 (1.83 ± 0.25 mm/year), ZK60/4β-TCP (1.63 ± 0.18 mm/year) and ZK60/12β-TCP (2.14 ± 0.34 mm/year).

In order to further study the effect of β-TCP on the degradation behavior, the corrosion surface of the soaked samples were studied by SEM (Figure 7). After immersed for 7 days, a compact film formed on the surface of the ZK60/8β-TCP composite, while loose corrosion product film with obvious cracks formed on the surface of the ZK60. As for the ZK60/12β-TCP, some huge gaps appeared in local areas on the surface. The EDS analysis indicated that the degradation products on ZK60 were mainly composed of Mg and O (Figure 7E), indicating a large amount of $Mg(OH)_2$ coated on the surface of ZK60. Significantly, large amounts of calcium and phosphorus were detected on the surface of the composite (Figure 7F). EDS revealed that the calcium/phosphate atom ratio of the product on the ZK60/8β-TCP composite was 1.617, which was close to that of apatite (1.67)[20]. Thus, it was reasonable to conclude that more apatite deposited on the surface of ZK60/*x*β-TCP composites. In addition, the deposition of apatite resulted in a more compact corrosion surface film on Mg matrix (Figure 7B and Figure 7C).

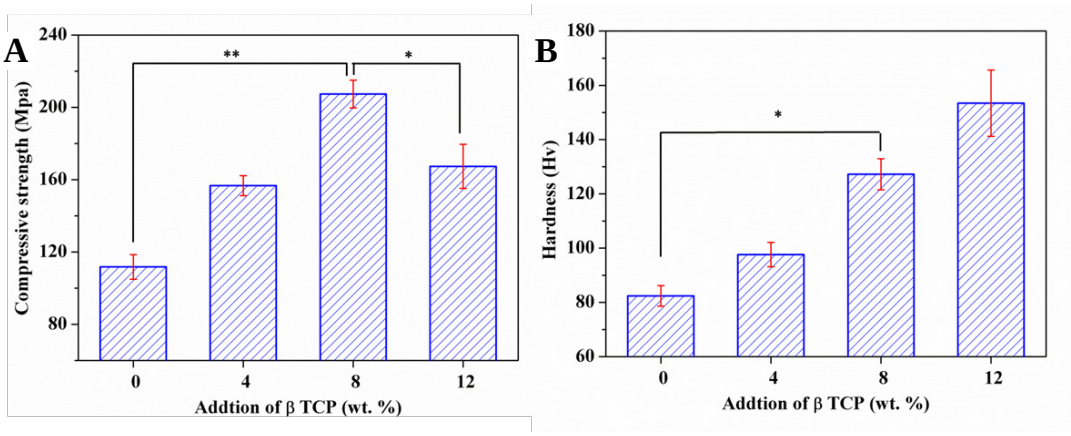

Figure 5. The (**A**) compressive strength and (**B**) hardness of the ZK60/xβ-TCP composites. ($n = 3$, $^*p < 0.05$, $^{**}p < 0.01$).

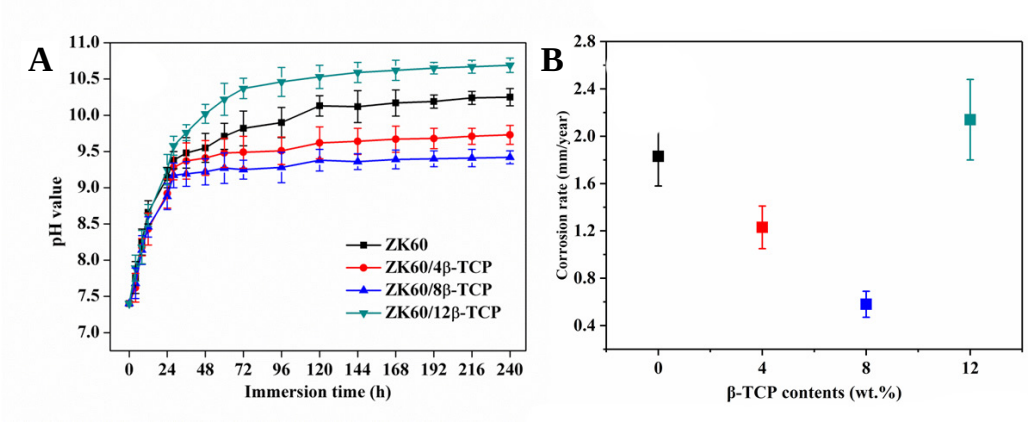

Figure 6. (**A**) The pH variation of SBF after immersion of ZK60/xβ-TCP composites and (**B**) calculated corrosion rate based on weight loss.

3.4 *In Vitro* Cell Response

Fluorescent images of the live/dead assay were presented in Figure 8. Live cells were indicated by the fluorescent green, while dead cells were indicated by the fluorescent red. It could be observed that cells cultured in the extracts of ZK60/8β-TCP presented a typical fusiform shape after 1 day culture (Figure 8C), suggesting their normal cell growth. As a comparison, cells cultured in ZK60 and ZK60/12β-TCP clearly showed a contraction of round shape (Figure 8A and Figure 8D), indicating its unhealthy growth. Meanwhile, a few of dead cells were observed for ZK60 and ZK60/12β-TCP. It should be noted that both ZK60/4β-TCP and ZK60/8β-TCP presented more live cells compared with ZK60 specimens, indicating an improved cytocompatibility of incorporating β-TCP into ZK60.

CCK-8 assay was used to determine the cell viability as a function of culture time, with results shown in Figure 9. Obviously, the cell activity gradually increased with the culture time increasing for all groups. At days 1, 3 and 5, significant differences in O.D. values ($p < 0.05$) were observed between ZK60/8β-TCP and ZK60. Besides, all the ZK60/*x*β-TCP composites exhibited higher O.D. values than ZK60, indicating better cell viability. Clearly, ZK60/8β-TCP showed higher cell viability than ZK60, ZK60/4β-TCP and ZK60/12β-TCP.

4. 4. Discussion

4.1 The Effect of Laser Rapid Solidification on Microstructure

Laser melting technology is able to process various biomaterials, including bioceramics and biometals. Nevertheless, bioceramics, such as hydroxyapatite, TCP and 45s bioglass, exhibit a too low mechanical strength for bone implant. Furthermore, bioceramic usually has a high viscosity and low fluidity, which impaired the density of laser processed part[21]. While Mg alloys exhibit suitable mechanical strength but poor corrosion resistance. Thus, substantial efforts have been devoted to fabricating bioceramic reinforced Mg alloys as candidates for bone implants. For instance, some researchers had fabricated β-TCP reinforced Mg-based

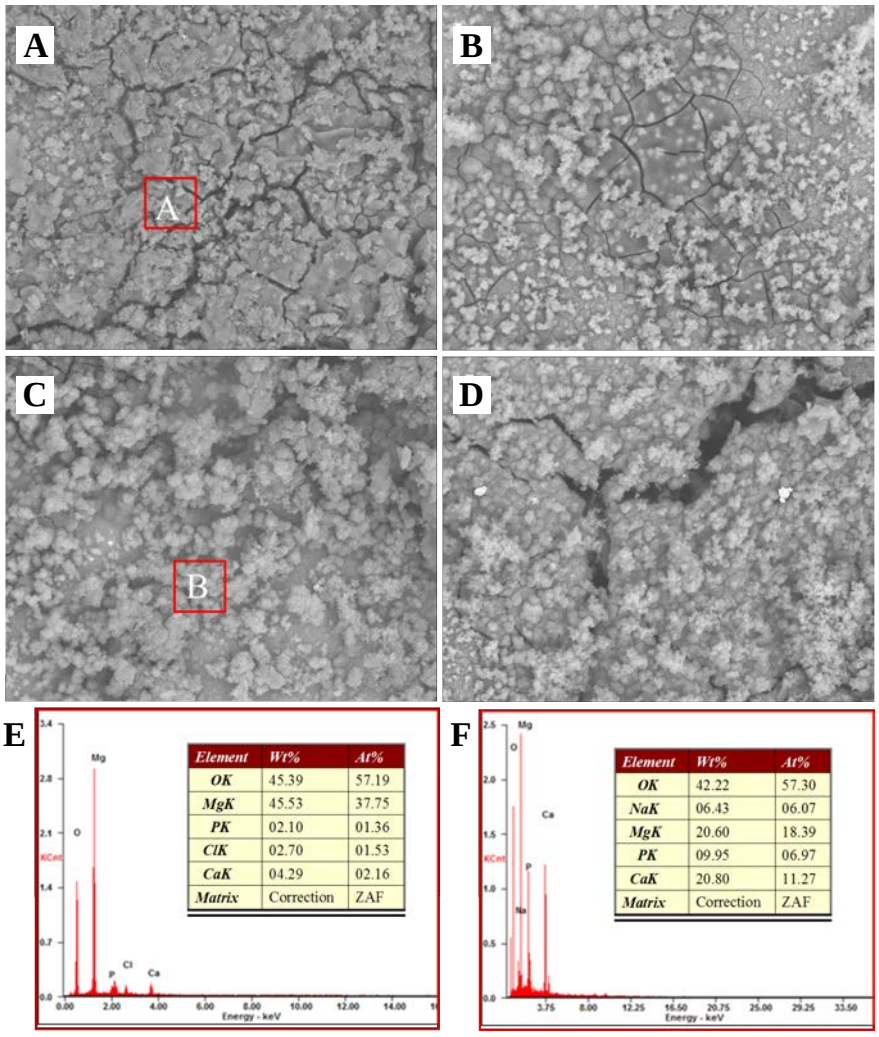

Figure 7. Corrosion surface of laser rapidly solidified ZK60/xβ-TCP composites: (**A**) ZK60; (**B**) ZK60/4β-TCP; (**C**) ZK60/8β-TCP; and (**D**) ZK60/12β-TCP. (**E**) EDS results of region A; (**F**) EDS results of region B.

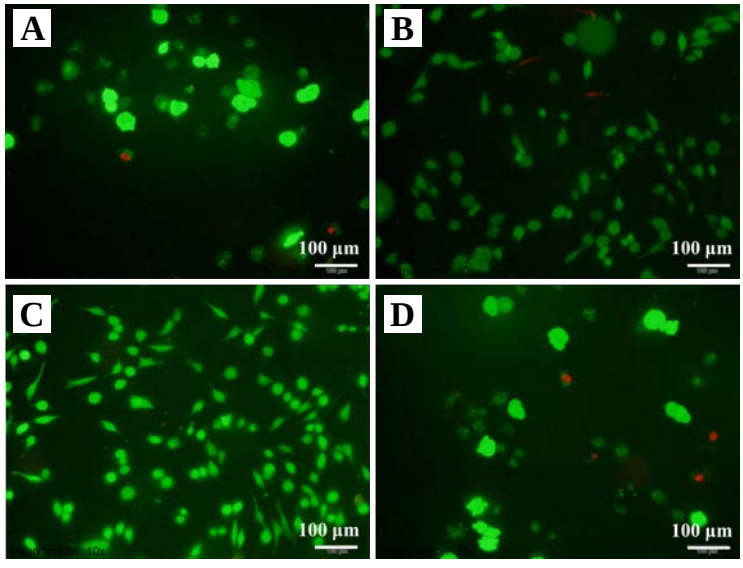

Figure 8. Fluorescence micrograph of live/dead dye-stained MG-63 cells after 1 day culture in the extracts of ZK60/xβ-TCP. (**A**) ZK60, (**B**) ZK60/4β-TCP, (**C**) ZK60/8β-TCP and (**D**) ZK60/12β-TCP.

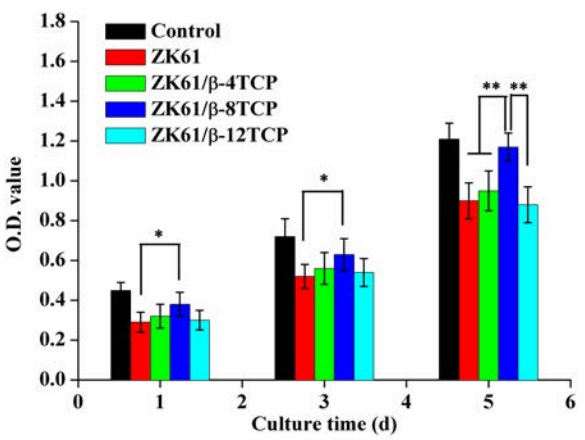

Figure 9. CCK-8 assay for MG-63 cells cultured in the extracts of ZK60/xβ-TCP composites for 1, 3 and 5 days. ($n = 3$, $*p < 0.05$, $**p < 0.01$).

composites by conventional techniques. Unfortunately, agglomeration phenomenon of β-TCP occurred even at a low content of 1.5 wt. % in casting process[11]. Huang *et al.*[22] reported that β-TCP aggregated in the matrix of casted Mg–2Zn–0.5Ca/1β-TCP at a lower content of 1 wt. %. Yan *et al.*[23] fabricated a kind of Mg-Zn/β-TCP composite by powder metallurgy, and also observed the aggregation of β-TCP in Mg matrix. The physical differences between β-TCP and α-Mg would be used to explain the agglomeration of β-TCP in the Mg matrix. β-TCP possessed a rhombohedral structure (lattice parameters a, b = 1.04352 nm, c = 3.7403 nm, a, β = 90° and γ = 120°), while α-Mg had a hexagonal structure (lattice parameters a, b = 0.32092 nm and c = 0.52105 nm)[24]. According to the heterogeneous nucleation theory, such a difference in crystal structure made it extremely difficult for α-Mg to nucleate on the surfaces of β-TCP particles. Thus, most of the β-TCP particles would be pushed by the growing front of α-Mg grains during the solidification. In equilibrium solidification with a low cooling rate, the β-TCP particles would be squeezed out continuously by slowly-advancing solid/liquid interfaces, finally gathered at the crystal interface and caused component segregation.

Combined processes have been reported to overcome the agglomeration of β-TCP in Mg matrix. For example, a melt shearing technology combined with high-pressure die casting was applied to fabricated β-TCP/Mg composite[12]. Besides, powder metallurgy, hot extrusion and aging treatment were combined to fabricated β-TCP/Mg-Zn composites[23]. In this study, laser rapid solidification, as one step process, was proposed to solve the problem. SEM images clearly showed that β-TCP homogeneously distributed along grains boundaries in Mg matrix, with β-TCP contents up to 8 wt. % (Figure 2). In laser rapid solidification, the velocity of the solid/liquid interface was extremely high, which was believed to be far faster than the movement of β-TCP particles. In this condition, the β-TCP particles would be captured by the solid/liquid interface and remained the original uniform distribution. On the other hand, laser rapid solidification could also cause a grain refinement with a high density of grains boundaries[6]. More grain boundaries would provide more distribution space for β-TCP particles, thus avoiding the aggregation of β-TCP particles.

4.2 The Effect of β-TCP on Mechanical Properties

Mechanical tests revealed that the incorporation of β-TCP significantly improved the compressive strength and hardness of ZK60. The increased compressive strength of ZK60/*x*β-TCP composites was due to: (I) a good interface bonding between the α-Mg grains and β-TCP particles gave rise to effective load transfer from α-Mg matrix to β-TCP particles, which possessed better load-bearing capacity[25]; (II) the homogeneously distributed β-TCP would serve as an obstacle to the dislocation movement and then ended up with dislocation pile ups; (III) the addition of β-TCP particles as second phase inhibited the growth of α-Mg grains, resulting in fine grain strengthening. However, the compressive strength of the ZK60/*x*β-TCP composites decreased with β-TCP further increasing to 12 wt. %. For ZK60/12β-TCP, excess β-TCP aggregated at the grain boundaries and formed coarsened second phase, which weakened the bonding interface between the α-Mg grains and adjacent β-TCP particles. A large number of pores and defects formed in the matrix, thus reducing the compressive strengths of the composite. Besides, the enhanced hardness was primarily attributed to that hard β-TCP particles acted as reinforcement phases, which impeded the dislocation movement.

4.3 The Effect of β-TCP on Degradation Behavior

It was well known that Mg had a lively chemical property. As Mg based alloys were exposed to aqueous solution, Mg would degrade according to the following chemical reactions[26]:

$$\text{Anodic: } Mg \rightarrow Mg^{2+} + 2e^{-} \quad (4.1)$$

$$\text{Cathodic: } 2H_2O + 2e^{-} \rightarrow H_2\uparrow + 2OH^{-} \quad (4.2)$$

$$\text{Product formation: } Mg^{2+} + 2OH^{-} \rightarrow Mg(OH)_2\downarrow \quad (4.3)$$

Hence a heavy layer of $Mg(OH)_2$, which exhibited a porous structure, was observed on the surface of ZK60 (Figure 7A). Meanwhile, the Cl^- ions contained in SBF could transformed $Mg(OH)_2$ into resoluble $MgCl_2$ as follows[16]:

$$Mg(OH)_2 + 2Cl^{-} \rightarrow MgCl_2 + 2OH^{-} \quad (4.4)$$

Thus, the coated $Mg(OH)_2$ layer could not provide an effective protection for the inner fresh Mg matrix from further degradation. Compared with ZK60, ZK60/8β-TCP had an enhanced corrosion resistance. This could be confirmed by the reduced pH value of SBF after immersion of ZK60/8β-TCP composite. The enhanced corrosion resistance of ZK60/8β-TCP was due to a more protective film formed on the corrosion surface. The β-TCP distributed in Mg matrix would dissolve in the aqueous solution as follows[27]:

$$3Ca_3(PO_4)_2 + H_2O \rightarrow HPO_4^{2-} + OH^{-} + 9Ca^{2+} + 5PO_4^{3-} \quad (4.5)$$

The released calcium ion and phosphate ion favored for the formation of apatite layer on surface. On the other hand, the β-TCP usually acted as the apatite nuclei leading to the deposition of apatite spontaneously[28]. Therefore, a large amount of apatite deposited on the surface and filled the pores of $Mg(OH)_2$ layer. As a result, a more compact surface film formed and effectively retarded the further degradation.

It should be noted that the corrosion rate accelerated as the β-TCP content increased up to 12 wt. %. This was because too much β-TCP aggregated at the grain boundaries and reduced the relative density of the matrix. As a consequence, the strongly corrosive Cl^- ion easily invaded into the matrix, which accelerated the degradation.

4.4 *In Vitro* Cell Response of ZK60/xβ-TCP

In the presented study, the extracts of ZK60/*x*β-TCP were utilized to mimic the environment during implantation. *In vitro* cell culture experiments indicated that MG-63 cells exhibited better growth in extracts of ZK60/8β-TCP than in that of ZK60. The improved cytocompatibility of ZK60/8β-TCP was believed to be closely related to the enhanced corrosion resistance. As shown in Figure 6A, the pH value significantly increased during the immersion due to the rapid degradation of Mg-based composites. In general, a weak alkaline environment with pH value ranging from 7.4 to 7.8 was more suitable for cell survival. An increased pH would significantly impair the enzyme activity, thus affecting the transport of substance for cell membrane. Meanwhile, a high pH value with high Mg^{2+} and OH^- concentration led to a too high osmotic pressure in culture medium[29]. Thus, the significantly increased pH had obvious inhibitory effects on cell proliferation. For ZK60/8β-TCP, the pH value and ion concentration (Mg^{2+}, OH^-) in culture medium were considerably reduced compared with ZK60, resulting in more appropriate pH value and osmolality for cell proliferation. Besides, the released Ca^{2+} caused by the degradation of β-TCP should also be responsible for the improvement of cytocompatibility for ZK60/8β-TCP. Ca, as a nutrient element for the human body, is essential in chemical signaling with cells[30]. Li *et al*. also reported that Ca^{2+} enhanced the proliferation of bone-derived cell[31]. Thus, the release of Ca^{2+} from ZK60/8β-TCP might exert a positive effect on the cell growth and proliferation.

5. Conclusions

In this study, β-TCP was composited with ZK60 *via* laser rapid solidification with an aim to improve the degradation behavior. It was revealed that laser rapid solidification restrained the segregation of β-TCP particles in Mg matrix. In addition, β-TCP particles uniformly distributed along grains boundaries in ZK60/8β-TCP. The results showed that the laser rapidly solidified ZK60/8β-TCP had an enhanced corrosion resistance and mechanical properties as compared with ZK60. Besides, the results of *in vitro* cell culture assays also revealed that ZK60/8β-TCP composite had an improved cytocompatibility to MG-63 cells. It was suggested that ZK60/8β-TCP was a potential biodegradable implant.

Conflict of Interest and Funding

No conflict of interest was reported by the authors. The authors gratefully acknowledge the following projects and funds for the financial support: (1) The Natural Science Foundation of China (51575537, 81572577, 51705540, 81472058); (2) Hunan Provincial Natural Science Foundation of China (2016JJ1027); (3) The Project of Innovation-driven Plan of Central South University (2016CX023); (4) The Open-End Fund for the Valuable and Precision Instruments of Central South University; (5) The fund of the State Key Laboratory of Solidification Processing at NWPU (SKLSP201605);

(6) The Project of State Key Laboratory of High Performance Complex Manufacturing, Central South University, and (7) National Postdoctoral Program for Innovative Talents (BX201700291).

References

1. Chen Y, Xu Z, Smith C, *et al*., 2014, Recent advances on the development of magnesium alloys for biodegradable implants. *Acta Biomater*, 10(11): 4561–4573. http://dx.doi.org/ 10.1016/j.actbio.2014.07.005
2. Tie D, Guan R, Liu H, *et al*., 2016, An *in vivo* study on the metabolism and osteogenic activity of bioabsorbable Mg–1Sr alloy. *Acta Biomater*, 29: 455–467. http://dx.doi.org/10.1016/j.actbio.2015.11.014
3. Yazdani M, Yazdani M, Afshar A, *et al*., 2017, Electrochemical evaluation of AZ 31 magnesium alloy in two simulated biological solutions. *Anti-Corros Method M*, 64(1): 103–108. http://dx.doi.org/10.1108/ACMM-02-2016-1649
4. Ge S, Wang Y, Tian J, *et al*., 2016, An *in vitro* study on the biocompatibility of WE magnesium alloys. *J Biomed Mater Res B Appl Biomater*, 104(3): 482–487. http://dx.doi.org/10.1002/jbm.b.33388
5. Feng A and Han Y, 2010, The microstructure, mechanical and corrosion properties of calcium polyphosphate reinforced ZK60A magnesium alloy composites. *J Alloys Compd*, 504(2): 585–593. http://dx.doi.org/10.1016/j.jallcom.2010.06.013
6. Shuai C, Yang Y, Wu P, *et al*., 2017, Laser rapid solidification improves corrosion behavior of Mg-Zn-Zr alloy. *J Alloys Compd*, 691: 961–969. https://doi.org/10.1016/j.jallcom.2016.09.019
7. Li N, Zheng Y, 2013, Novel magnesium alloys developed for biomedical application: A review. *J Mater Sci Technol*, 29(6): 489–502. https://doi.org/10.1016/j.jmst.2013.02.005
8. Del Campo R, Savoini B, Munoz A, *et al*., 2014, Mechanical properties and corrosion behavior of Mg–HAP composites. *J Mech Behav Biomed Mater*, 39: 238–246. https://doi.org/10.1016/j.jmbbm.2014.07.014
9. Wan Y, Cui T, Li W, *et al*., 2016, Mechanical and biological properties of bioglass/magnesium composites prepared *via* microwave sintering route. *Mater Des*, 99: 521–527. https://doi.org/10.1016/j.matdes.2016.03.096
10. Feng A and Han Y, 2011, Mechanical and *in vitro* degradation behavior of ultrafine calcium polyphosphate reinforced magnesium-alloy composites. *Mater Des*, 32(5): 2813–2820. https://doi.org/10.1016/j.matdes.2010.12.054
11. He S-Y, Yue S, Chen M-F, *et al*., 2011, Microstructure and properties of biodegradable β-TCP reinforced Mg-Zn-Zr composites. *Trans Nonferrous Met Soc China*, 21(4): 814–819. https://doi.org/10.1016/S1003-6326(11)60786-3
12. Liu D, Zuo Y, Meng W, *et al*., 2012, Fabrication of biodegradable nano-sized β-TCP/Mg composite by a novel melt shearing technology. *Mater Sci Eng C*, 32(5): 1253–1258. https://doi.org/10.1016/j.msec.2012.03.017
13. Yazdimamaghani M, Razavi M, Vashaee D, *et al*., 2016, *In vitro* analysis of Mg scaffolds coated with polymer/hydrogel/ceramic composite layers. *Surf Coat Technol*, 301: 126–132. https://doi.org/10.1016/j.surfcoat.2016.01.017
14. Xie D, Zhao J, Qi Y, *et al*., 2013, Decreasing pores in a laser cladding layer with pulsed current. *Chin Opt Lett*, 11(11): 111401. https://doi.org/10.3788/COL201311.111401.
15. Liang Y-J, Li J, Li A, *et al*., 2017, Solidification path of single-crystal nickel-base superalloys with minor carbon additions under laser rapid directional solidification conditions. *Scr Mater*, 127: 58–62. https://doi.org/10.1016/j.scriptamat.2016.08.039
16. Banerjee R, Collins P Cand Fraser H L, 2002, Laser deposition of *in situ* Ti–TiB composites. *Adv Eng Mater,* 4(11): 847–851. https://doi.org/10.1002/1527-2648(20021105)4:11<847::AID-ADEM847>3.0.CO;2-C
17. Yang Y, Wu P, Lin X, *et al*., 2016, System development, formability quality and microstructure evolution of selective laser-melted magnesium. *Virtual Phys Prototyp*, 11(3): 1–9. http://dx.doi.org/10.1080/17452759.2016.1210522
18. Pillai R S, Frasnelli M, Sglavo V M, 2017, HA/β-TCP Plasma Sprayed Coatings on Ti Substrate for Biomedical Applications. *Ceram Int*. https://doi.org/10.1016/j.ceramint.2017.08.113
19. Sutton A T, Kriewall C S, Ming C L, *et al*., 2016, Powder characterisation techniques and effects of powder characteristics on part properties in powder-bed fusion processes. *Virtual Phys Prototyp*, 12(1): 3–29. http://dx.doi.org/10.1080/17452759.2016.1250605
20. Ivanchenko P, Delgado-López J M, Iafisco M, *et al*., 2017, On the surface effects of citrates on nano-apatites:

Evidence of a decreased hydrophilicity. *Sci Rep*, 7:8901. http://dx.doi.org/10.1038/s41598-017-09376-x

21. Sing S L, Yeong W Y, Wiria F E, *et al*., 2017, Direct selective laser sintering and melting of ceramics: A review. *Rapid Prototyp J*, 23(3): 611–623. http://dx.doi.org/10.1108/RPJ-11-2015-0178
22. Huang Y, Liu D, Anguilano L, *et al*., 2015, Fabrication and characterization of a biodegradable Mg–2Zn–0.5 Ca/1β-TCP composite. *Mater Sci Eng C*, 54: 120–132. http://dx.doi.org/10.1016/j.msec.2015.05.035
23. Yan Y, Kang Y, Li D, *et al*., 2017, Improvement of the mechanical properties and corrosion resistance of biodegradable β-Ca_3 (PO_4) 2/Mg-Zn composites prepared by powder metallurgy: The adding β-Ca_3 $(PO_4)_2$, hot extrusion and aging treatment. *Mater Sci Eng C*, 74: 582–596. http://dx.doi.org/10.1016/j.msec.2016.12.132
24. Yashima M, Sakai A, Kamiyama T, *et al*., 2003, Crystal structure analysis of β-tricalcium phosphate $Ca_3(PO_4)_2$ by neutron powder diffraction. *J Solid State Chem*, 175(2): 272–277. http://dx.doi.org/10.1016/S0022-4596(03)00279-2
25. Garoushi S K, Hatem M, Lassila L V, *et al*., 2015, The effect of short fiber composite base on microleakage and load-bearing capacity of posterior restorations. *Acta Biomater Odontol Scand*, 1(1): 6–12. http://dx.doi.org/10.3109/23337931.2015.1017576
26. Agarwal S, Curtin J, Duffy B, *et al*., 2016, Biodegradable magnesium alloys for orthopaedic applications: A review on corrosion, biocompatibility and surface modifications. *Mater Sci Eng C*, 68: 948–963. http://dx.doi.org/10.1016/j.msec.2016.06.020
27. Geng F, Tan L, Jin X, *et al*., 2009, The preparation, cytocompatibility, and *in vitro* biodegradation study of pure β-TCP on magnesium. *J Mater Sci Mater Med*, 20(5): 1149–1157. http://dx.doi.org/10.1007/s10856-008-3669-x
28. Kokubo T, 1996, Formation of biologically active bone-like apatite on metals and polymers by a biomimetic process. *Thermochim Acta*, 280–281: 479–490. http://dx.doi.org/10.1016/0040-6031(95)02784-X
29. Zhang L, Pei J, Wang H, *et al*., 2017, Facile preparation of poly (lactic acid)/brushite bilayer coating on biodegradable magnesium alloys with multiple functionalities for orthopedic application. *ACS Appl Mater Interfaces*, 9(11): 9437–9448. http://dx.doi.org/10.1021/acsami.7b00209
30. Ilich J Z and Kerstetter J E, 2000, Nutrition in bone health revisited: A story beyond calcium. *J Am Coll Nutr*, 19(6): 715–737. http://dx.doi.org/10.1080/07315724.2000.10718070
31. Li Z, Gu X, Lou S, *et al*., 2008, The development of binary Mg–Ca alloys for use as biodegradable materials within bone. *Biomaterials*, 29(10): 1329–1344. http://dx.doi.org/10.1016/j.biomaterials.2007.12.021